Resistive Switching of Ta_2O_5-Based Self-Rectifying Vertical-Type Resistive Switching Memory

Sungyeon Ryu, Seong Keun Kim & Byung Joon Choi

Journal of Electronic Materials

ISSN 0361-5235
Volume 47
Number 1

Journal of Elec Materi (2018) 47:162-166
DOI 10.1007/s11664-017-5787-z

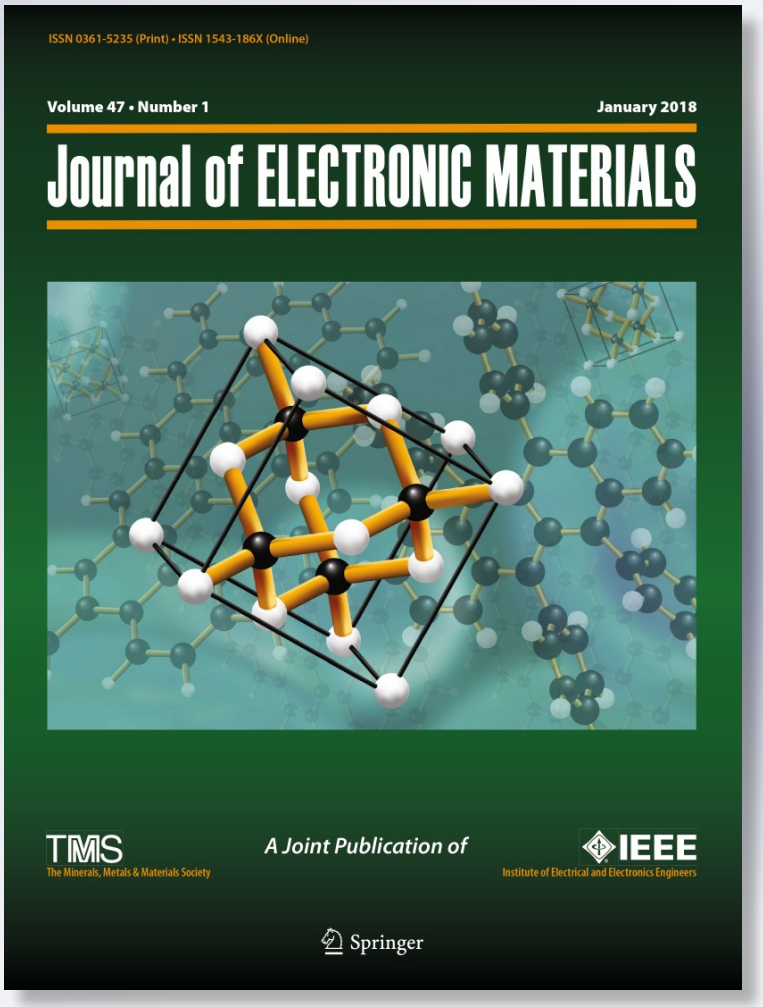

Springer

Journal of ELECTRONIC MATERIALS, Vol. 47, No. 1, 2018
DOI: 10.1007/s11664-017-5787-z

Resistive Switching of Ta_2O_5-Based Self-Rectifying Vertical-Type Resistive Switching Memory

SUNGYEON RYU,[1] SEONG KEUN KIM,[2] and BYUNG JOON CHOI[1,3]

1.—Department of Materials Science and Engineering, Seoul National University of Science and Technology, Seoul 01811, Republic of Korea. 2.—Center for Electronic Materials, Korea Institute of Science and Technology, 5 Hwarang-ro 14-gil, Seongbuk-gu, Seoul 02792, Republic of Korea. 3.—e-mail: bjchoi@seoultech.ac.kr

To efficiently increase the capacity of resistive switching random-access memory (RRAM) while maintaining the same area, a vertical structure similar to a vertical NAND flash structure is needed. In addition, the sneak-path current through the half-selected neighboring memory cell should be mitigated by integrating a selector device with each RRAM cell. In this study, an integrated vertical-type RRAM cell and selector device was fabricated and characterized. Ta_2O_5 as the switching layer and TaO_xN_y as the selector layer were used to preliminarily study the feasibility of such an integrated device. To make the side contact of the bottom electrode with active layers, a thick Al_2O_3 insulating layer was placed between the Pt bottom electrode and the Ta_2O_5/TaO_xN_y stacks. Resistive switching phenomena were observed under relatively low currents (below 10 μA) in this vertical-type RRAM device. The TaO_xN_y layer acted as a nonlinear resistor with moderate nonlinearity. Its low-resistance-state and high-resistance-state were well retained up to 1000 s.

Key words: Resistive switching, vertical-type resistive random access memory, self-rectifying, conducting filament

INTRODUCTION

Resistive switching random-access memory (RRAM) devices have been considered promising non-volatile memory devices because of their simple structure,[1,2] fast operation time,[3] lower power consumption,[4] sufficient switching endurance,[5] and excellent scalability.[6] Various kinds of materials, such as oxides, nitrides, and sulfides, have been used as resistive switching layers.[5,7–11] Tantalum oxide-based RRAM devices in particular have many competitive properties, such as high endurance up to 10^{12} cycles,[5] switching rates down to sub-nanoseconds,[12] low operating energies,[13] and so on.

It is thought that RRAM devices can be vertically stacked in a manner similar to that of vertical NAND flash memory, which can be considered a 90° rotation of a horizontally stacked crossbar array. This type of architecture, the so-called vertical-type RRAM, can reduce the large number of lithographic processes usually used, as well as the fabrication cost. In the vertical-type RRAM, the edges of multiple layers of metal electrodes separated by dielectric layers should form metal–insulator–metal (MIM) junctions. In addition, each RRAM cell must be integrated with a selector device that shows nonlinear current (I)–voltage (V) characteristics to mitigate a sneak-path current issue,[14] where unselected or half-selected memory cells do not operate under $1/2V_{read}$ or $1/2V_{write}$ in the crossbar arrays.

So far, such an integrated RRAM cell and selector device to form vertical-type RRAM has rarely been reported. As a preliminary work for understanding the electrical properties of vertical-type RRAM, single and double layers of the metal electrode edge-contact memory elements were studied. Lee et al.[15] reported the fabrication of double layers of graphene for an edge-contact HfO_x film. The vertically formed TiN/HfO_x/graphene stack showed repeatable resistive switching at quite low

(Received March 18, 2017; accepted September 1, 2017; published online September 14, 2017)

switching voltage (±0.2 V) and current (~2 μA) levels. Bai et al.[16] reported reactive sputter-grown three-layer 3-D vertical $AlO_\delta/Ta_2O_{5-x}/TaO_y$ RRAM cells exhibiting 4-level resistance states. Yoon et al.[17] recently reported resistive switching behavior in a vertical contact $Pt/Ta_2O_5/HfO_2/TiN$ stack. Atomic layer-deposited (ALD) Ta_2O_5/HfO_2 films exhibited form-free and self-rectifying resistive switching behavior and low current operation (below 10 nA). Although no selector device was adapted in the aforementioned works, the interfacial resistance between the materials (for the graphene/HfO_x) or a high Schottky barrier (for the Pt/Ta_2O_5) was believed to provide moderate selectivity. The absence of an individual selector device is highly desirable in terms of fabrication complexity; however, these electrode materials and nonfilamentary-type multiple switching layers are not considered yet in industry.

In this study, we fabricated a vertical-type RRAM device made of Ta_2O_5 as the switching element and TaO_xN_y as the selector element. ALD-grown TaN_x or TaO_xN_y films showed nonlinear *I–V* characteristics under the Poole–Frenkel electrical conduction mechanism. ALD could be highly beneficial to simplify the fabrication process of 3-dimensional integration of memory cell for both switching and selector elements. Low switching currents (< 10 μA) and good retention properties were observed in these vertical-type RRAM devices. Especially triple-state resistive switching was induced by DC bias, and the reason for such a phenomenon was considered in terms of conducting filament formation.

EXPERIMENT

The RRAM device was fabricated on thermally grown silicon dioxide on a silicon substrate. For a crosspoint device, a 100-nm-thick Pt bottom electrode and a 50-nm-thick AlO_x insulating layer were sequentially deposited by electron (e)-beam evaporation on a photolithographical pattern for the lift-off process. In the following, the dumbbell shape of the bottom electrode with an AlO_x insulating layer on it was formed by removing the sacrificial pattern. Then, a 5-nm-thick TaO_xN_y selector layer and a 5-nm-thick Ta_2O_5 switching layer were deposited by plasma-enhanced ALD. The Ta_2O_5 layer was deposited using a tetra-butylimido tris(dimethylamido) tantalum (TBTMET) precursor and O_2 plasma gas. The TaO_xN_y layer was grown as a $TaN_x/Ta_2O_5/TaN_x$ tri-layer using the same Ta precursor and a mixed plasma gas of N_2 and H_2 for TaN_x and O_2 plasma gas for Ta_2O_5, respectively. Then, a 20-nm-thick Pt top electrode was deposited by e-beam evaporation to form a crossbar device by the lift-off process. Figure 1a shows a schematic of the device and the DC measurement system, and Fig. 1b shows the optical image of the device. The width of the electrode was 2 μm, and; thus, the nominal device area was approximately 0.2 μm^2 (2 μm × 100 nm).

The DC *I–V* and retention characteristics of the device were measured using a semiconductor parameter analyzer (SPA, HP-4156) at room temperature. To examine the microstructure and chemical properties of the device, transmission electron microscopy (TEM, JEM-2100F, JEOL/CEOS) analysis combined with energy-dispersive spectroscopy (EDS) was performed after cross-sectioning using a focused ion beam (FIB, NOVA 600 Nanolab, FEI).

RESULTS AND DISCUSSION

Typical DC *I–V* loops of the vertical-type RRAM made of a $Pt/Ta_2O_5/TaO_xN_y/Pt$ stack with an area of 0.2 μm^2 are shown Fig. 2. The as-fabricated state of the device was highly resistive. By applying a positive bias voltage on the top electrode, the device could be transitioned to a low-resistance state (LRS) at 4.5 V, which is a SET operation. An electroforming process was not required in this device. The next positive voltage sweep showed that such a resistance state was maintained up to 4 V. A negative bias voltage was then applied, and the resistance state changed to a high-resistance state (HRS) at −3 V, that is a RESET operation. Then, the non-volatility of the resistance state was confirmed by negative voltage sweeps up to −4 V. It is noted that the current for both transitions was not limited by current compliance; the maximum switching current was below 10 μA. In addition, a high resistance ratio ($R_{HRS}/R_{LRS} \approx 10^4$) was observed.

Interestingly, this vertical-type RRAM device showed the feasibility of multi-bit operation. To examine the multiple resistance states, the maximum positive bias voltage was increased to 12 V. The device was changed to LRS1 first at approximately 4 V and then to an even lower resistance state (LRS2) at approximately 12 V, as shown in Fig. 3. Both LRS1 and LRS2 abruptly reversed to HRS by applying a negative voltage sweep. These results show that the device had at least three resistance states: HRS, LRS1, and LRS2. Here, LRS1 is the same resistance state as LRS in Fig. 2. The non-volatility of each resistance state was also confirmed. The switching voltages from LRS2 to HRS and from LRS1 to HRS were almost the same because most of the voltage was applied to the resistive switching element once the transition from LRS2 to LRS1 occurred, which directly induced the transition from LRS1 to HRS.

To understand the microstructure of the device, TEM-EDS analysis was conducted after cross-sectioning of the device by FIB. As shown in the inset of Fig. 1b, the line profile of the element was acquired through the horizontal direction. Figure 4 shows the magnified TEM image (upper panel) and corresponding chemical profiles (lower panel) of each element (Ta, Pt, N, and O). According to the TEM image and elemental profiles, the ALD-grown Ta_2O_5/TaO_xN_y layers were well deposited in the sidewall of the Pt bottom electrode. The large

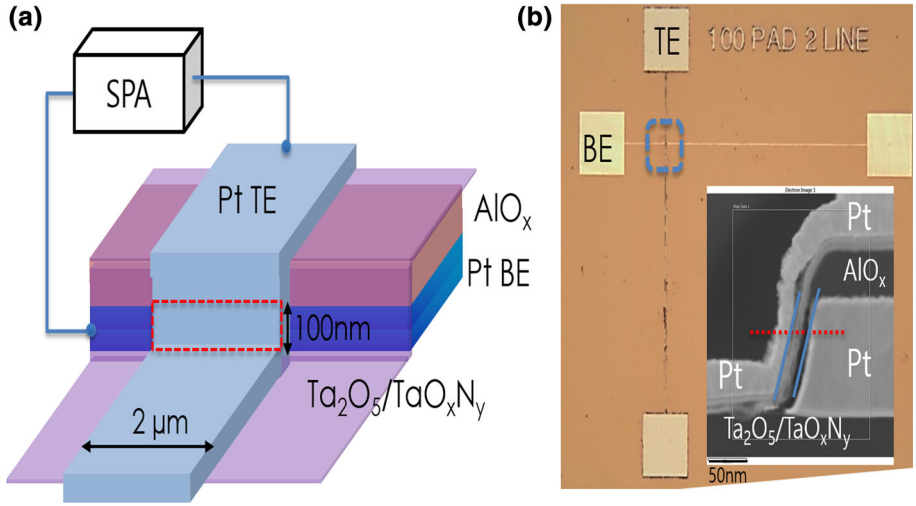

Fig. 1. (a) Schematic diagram of the vertical-type RRAM device and measurement system and (b) optical microscopic image of the crossbar device (inset: TEM image of the cross-section of the device).

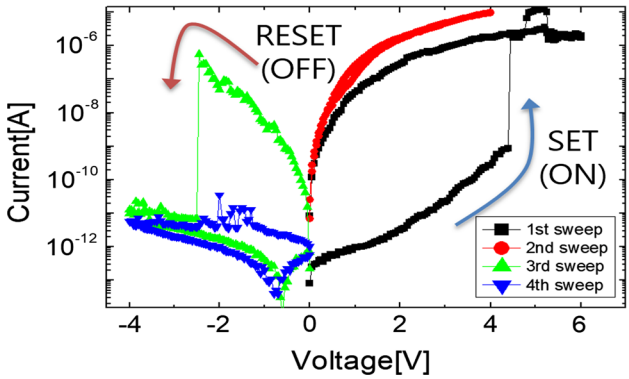

Fig. 2. Initial DC *I–V* characteristics of the device showing forming, RESET, and SET switching.

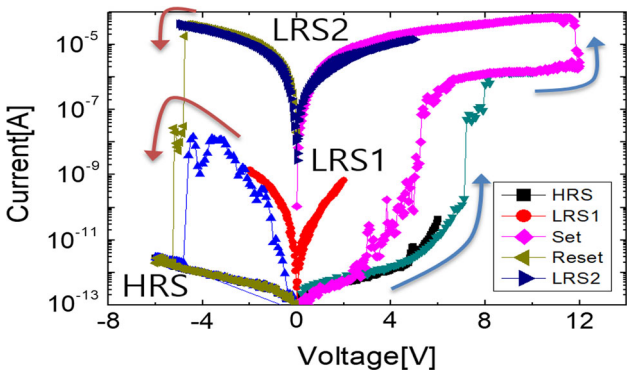

Fig. 3. Demonstration of three resistance states by DC *I–V* sweep.

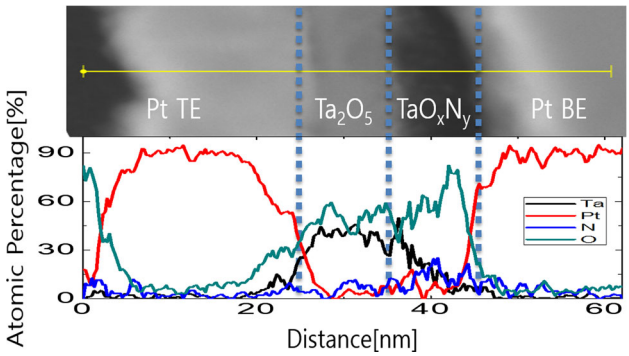

Fig. 4. TEM image of cross-section of the device (upper panel) and element line profiles (lower panel).

amount of oxygen in the TaO_xN_y layer may be attributed to the delamination of the layer from the Pt bottom electrode owing to poor adhesion and gas bubbling during the electrical manipulation.

The reason for the three resistance states could be explained by the so-called hourglass-shaped conducting filament (CF) model.[18,19] Figure 5a–d show schematic diagrams of the initial state and LRS1, LRS2, and HRS, respectively, in the device. In Fig. 5a, it is considered that oxygen vacancies already exist at the Ta_2O_5/TaO_xN_y interface because the metallic TaN_x surface of the TaO_xN_y layer ($TaN_x/Ta_2O_5/TaN_x$ tri-layer) attracts oxygen from the Ta_2O_5 layer. When a positive bias voltage is applied to the top electrode, positively charged oxygen vacancies migrate to the bottom electrode, whereas newly generated oxygen vacancies (which may form a CF) at the top electrode interface may move to the counter electrode, as shown schematically in Fig. 5b. Oxygen vacancies at the bottom electrode should also be retracted, but the retraction rate is slower than the growth rate of CF from the topside because the electric field is less concentrated at the bottom electrode. Once the CF at the topside is close to the bottom interface, the resistance state is gradually reduced to LRS1 (+4.5 V). When a higher voltage is applied (+12 V), an even wider CF can be fully connected between the two electrodes,

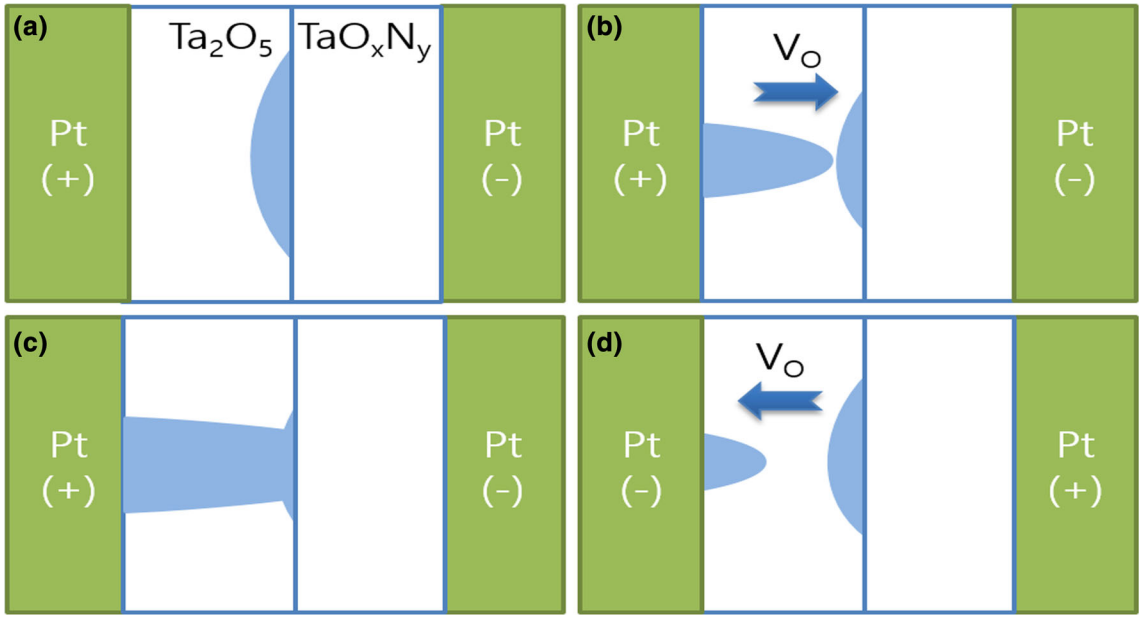

Fig. 5. Schematic diagrams of switching mechanism in the device: (a) initial state, (b) LRS1, (c) LRS2, and (d) HRS.

as shown schematically in Fig. 5c. This resistance state then becomes LRS2. The direction of the CF growth and retraction is completely reversed under negative voltage bias, that is, the topside CF rapidly moves back as compared to the movement of oxygen vacancies at the bottom interface. Therefore, the CF is abruptly disconnected (−4 V) and the resistance state of the device is changed to HRS, which is shown schematically in Fig. 5d.

It was supposed that the TaO_xN_y layer might play an important role as a selector device. However, there are two reasons why the TaO_xN_y layer does not seem to work as supposed: (1) The blocking (middle) electrode between Ta_2O_5/TaO_xN_y may not be inserted, and thus a single Schottky barrier at the TaO_xN_y/Pt interface may not be enough to rectify the current conduction; and (2) inter-diffusion between the Ta_2O_5/TaO_xN_y layers may have occurred, and so the TaO_xN_y layer may act as an electrical nonlinear resistor and oxygen ionic reservoir rather than as an isolated selector device.

Lastly, the stability of each resistance state was examined. Figure 6 shows the retention properties of those resistance states. A reading voltage (1 V) was applied to monitor the resistance state up to 1000 s. The subsequent resistance values of HRS, LRS1, and LRS2 were approximately 10^{13}, 10^{10}, and 10^7 Ω, respectively. The retention of HRS was difficult to measure using the short-pulse mode, unlike those of LRS1 and LRS2, because the current detection limit of the retention test was approximately 10 pA. Therefore, the DC *I–V* value was measured up to 1 V to get the resistance of HRS. Each resistance state was well retained during the retention test, without degradation.

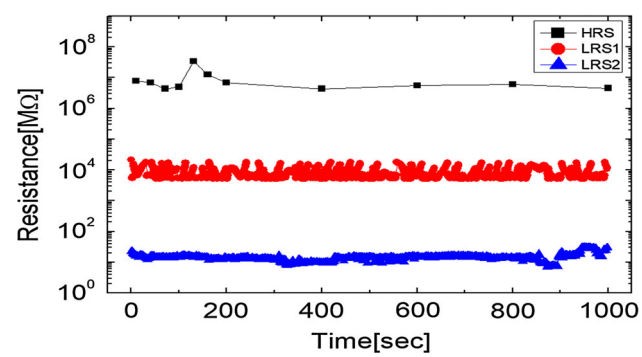

Fig. 6. Retention characteristics of three resistance states of the device.

CONCLUSION

In this study, a Ta_2O_5-based vertical-type RRAM device was fabricated and its resistive switching characteristics were investigated. The device showed low current operation and a high resistance ratio. In addition, three resistance states were achieved in two steps of the SET operation, whereas the RESET process occurred once. The hourglass-shaped CF model was applied to explain the self-rectifying resistive switching behavior. Each resistance state was well retained during the retention test. This work may be considered the first step toward realizing Ta_2O_5-based vertical-type RRAM devices utilized by an ALD process for high-density memory in the next generation.

ACKNOWLEDGEMENT

This research was supported by Basic Science Research Program through the National Research Foundation of Korea (NRF) funded by the Ministry

of Education (2014R1A1A2054597) and Nano Material Technology Development Program through the National Research Foundation of Korea (NRF) funded by the Ministry of Science, ICT and Future Planning (2009-0082580).

REFERENCES

1. R. Waser and M. Aono, *Nat. Mater.* 6, 833 (2007).
2. R. Waser, R. Dittmann, G. Staikov, and K. Szot, *Adv. Mater.* 21, 2632 (2009).
3. H.Y. Lee, P.S. Chen, T.Y. Wu, Y.S. Chen, C.C. Wang, P.J. Tzeng, C.H. Lin, F. Chen, C.H. Lien, and M.J. Tsai, in *IEDM Conference Proceedings* (2008), p. 297.
4. M. Wu, Y. Lin, W. Jang, and C. Lin, *IEEE Electron Device Lett.* 32, 1026 (2011).
5. M. Lee, C.B. Lee, D. Lee, S.R. Lee, M. Chang, J.H. Hur, Y. Kim, C. Kim, D.H. Seo, S. Seo, U. Chang, I. Yoo, and K. Kim, *Nat. Mater.* 10, 625 (2011).
6. B. Govoreanu, G.S. Kar, Y. Chen, V. Paraschiv, S. Kubicek, A. Fantini, I.P. Radu, L. Goux, S. Clima, R. Degraeve, N. Jossart, O. Richard, T. Vandeweyer, K. Seo, P. Hendrickx, G. Pourtois, H. Bender, L. Altimime, D.J. Wouters, J.A. Kittl, and M. Jurczak, in *IEDM Conference Proceedings*, vol. 11 (2011), pp. 729–732.
7. Y.C. Yang, F. Pan, Q. Liu, M. Liu, and F. Zeng, *Nano Lett.* 9, 1636 (2009).
8. Q. Liu, W. Guan, S. Long, R. Jia, and M. Liu, *Appl. Phys. Lett.* 92, 012117 (2008).
9. J.J. Yang, M.D. Pickett, X. Li, D.A.A. Ohlberg, D.R. Stewart, and R.S. Williams, *Nat. Nanotechnol.* 3, 429 (2008).
10. H.Y. Jeong, J.Y. Lee, M. Ryu, and S. Choi, *Phys. Status Solidi RRL* 4, 28 (2010).
11. S.Y. Choi, M.K. Yang, S. Kim, and J. Lee, *Phys. Status Solidi RRL* 4, 359 (2010).
12. A.C. Torrezan, J.P. Strachan, G.M. Ribeiro, and R.S. Williams, *Nanotechnology* 22, 485203 (2011).
13. J.J. Yang, M.X. Zhang, J.P. Strachan, F. Miao, M.D. Pickett, R.D. Kelley, G.M. Ribeiro, and R.S. Williams, *Appl. Phys. Lett.* 97, 232102 (2010).
14. J. Borghetti, G.S. Snider, P.J. Kuekes, J.J. Yang, D.R. Stewart, and R.S. Williams, *Nature* 464, 873 (2010).
15. S. Lee, J. Sohn, Z. Jiang, H.Y. Chen, and H.P. Wong, *Nat. Commun.* 6, 8407 (2015).
16. Y. Bai, H. Wu, R. Wu, Y. Zhang, N. Deng, Z. Yu, and H. Qian, *Sci. Rep.* 4, 5780 (2014).
17. J.H. Yoon, S. Yoo, S.J. Song, K.J. Yoon, D.E. Kwon, Y.J. Kwon, T.H. Park, H.J. Kim, X.L. Shao, Y. Kim, C.S. Hwang, and A.C.S. Appl, *Mater. Inter.* 8, 18215 (2016).
18. R. Degraeve, A. Fantini, N. Raghavan, L. Goux, S. Clima, Y.Y. Chen, A. Belmonte, S. Cosemans, B. Govoreanu, D.J. Wouters, P. Roussel, G.S. Kar, G. Groeseneken, and M. Jurczak, in *IPFA Conference Proceedings* (2014), pp. 245–249.
19. T.H. Park, S.J. Song, H.J. Kim, S.G. Kim, S. Chung, B.Y. Kim, K.J. Lee, K.M. Kim, B.J. Choi, and C.S. Hwang, *Sci. Rep.* 5, 15965 (2015).